(Preprint) AAS 19-222

INSIGHT ATTITUDE CONTROL SYSTEM THRUSTER CHARACTERIZATION AND CALIBRATION FOR SUCCESSFUL NAVIGATION TO MARS

Jill Seubert,* Eric D. Gustafson,† C. Allen Halsell,‡ Dale Howell,§ Thomas Kennedy,¶ Julim Lee,‖ and Sarah Elizabeth McCandless**

In order for the InSight spacecraft to execute a safe Mars landing, it was crucial that the navigation team accurately predict the trajectory and deliver the spacecraft to the targeted atmospheric entry point. One of the primary challenges faced by the Navigation Team was the accurate reconstruction and prediction of small but frequent velocity changes imparted by the spacecraft's Attitude Control System thrusters. This paper discusses the in-flight thruster calibration campaign, the reconstruction and prediction of accelerations throughout various phases of cruise (including compensating for significant outgassing after launch and attitude transition), and the subsequent impact on atmospheric entry point delivery.

INTRODUCTION

The InSight spacecraft launched from Vandenberg Air Force Base on May 5, 2018, and following a seven-month cruise landed on Mars on November 26, 2018. InSight carried significant heritage from the 2007 Mars Phoenix Lander Mission, including the unguided lander system. This required accurate delivery of the spacecraft to a predetermined atmospheric entry point with an entry flight path angle of -12.0° ± 0.21° (3-σ) to maximize the probability of a safe landing. One of the primary navigation challenges faced by the InSight Navigation Team was the accurate reconstruction and prediction of small but frequent velocity changes imparted by the spacecraft's Attitude Control System (ACS). Like Phoenix, the InSight spacecraft was three-axis stabilized via an unbalanced thruster control system, with the ACS Reaction Control System (RCS) thrusters being fired intermittently to maintain a fixed deadband attitude profile; the accumulation of these firings over the seven month cruise significantly impacted the spacecraft trajectory. Proper in-flight characterization of these thruster firings, often referred to as small forces, has proven to be crucial to the successful

*Orbit Determination Analyst, Mission Design and Navigation Section, NASA Jet Propulsion Laboratory, California Institute of Technology, 4800 Oak Grove Drive, Pasadena, CA 91109.

†Orbit Determination Lead, Mission Design and Navigation Section, NASA Jet Propulsion Laboratory, California Institute of Technology, 4800 Oak Grove Drive, Pasadena, CA 91109.

‡Navigation Team Chief, Mission Design and Navigation Section, NASA Jet Propulsion Laboratory, California Institute of Technology, 4800 Oak Grove Drive, Pasadena, CA 91109.

§Guidance and Control Engineer, Lockheed Martin Corporation, 8000 Southpark Way, Bldg 2, Littleton, CO 80120.

¶Guidance and Control Engineer, Lockheed Martin Corporation, 8000 Southpark Way, Bldg 2, Littleton, CO 80120.

‖Orbit Determination Analyst, Mission Design and Navigation Section, NASA Jet Propulsion Laboratory, California Institute of Technology, 4800 Oak Grove Drive, Pasadena, CA 91109.

**Orbit Determination Analyst, Mission Design and Navigation Section, NASA Jet Propulsion Laboratory, California Institute of Technology, 4800 Oak Grove Drive, Pasadena, CA 91109.

navigation of numerous interplanetary spacecraft, including 2001 Mars Odyssey, 2005 Mars Reconnaissance Orbiter, 2007 Mars Phoenix Lander, and Stardust comet sample return missions, as well as to the loss of the 1999 Mars Climate Observer.[1–6] Further complicating the trajectory prediction, the spacecraft experienced a high level of outgassing during early cruise, likely due to the launch slip from March 2016 to May 2018. In order to maintain the nominal spacecraft attitude in the presence of this large perturbation, the RCS thrusters fired at a significantly higher rate than was anticipated pre-launch.

The attitude and small force telemetry generated by the spacecraft's ACS was routinely processed to provide an *a priori* model of the spacecraft dynamics within the data arc and to generate predictive models of the average RCS thruster accelerations. To enhance the RCS thruster small force characterization, the spacecraft team performed a mid-cruise calibration of the four RCS attitude control thrusters. During the calibration activity, the spacecraft executed a sequence of RCS thruster firings in specific attitudes chosen to maximize observability of all thruster axes, to the extent constrained by vehicle thermal and communication considerations.[7] Deep Space Network tracking data and telemetered gyroscope data from the spacecraft's inertial measurement unit was processed using an Unscented Kalman Filter to obtain increased knowledge of the thrusters' flight performance relative to the pre-launch nominal values. This paper presents an overview of the InSight ACS system and available telemetry, and discusses the RCS system response throughout cruise, empirical prediction of thruster accelerations, the formulation and results of the thruster calibration campaign, and the impact of proper characterization and prediction of the RCS thruster firings on the atmospheric entry point delivery.

ATTITUDE CONTROL SYSTEM OVERVIEW

Attitude Control System

The InSight ACS was very similar to that of the Phoenix spacecraft, which landed on Mars on May 25, 2008.[1] The ACS consisted of star trackers, two Inertial Measurement Units (MIMUs), and Sun sensors. The Sun sensors served as backup attitude determination sensors, with the star trackers and MIMUs providing the primary spacecraft pointing information. Like Phoenix, an unbalanced thruster control system consisting of four Reaction Control System (RCS) thrusters was utilized to provide three-axis stabilization of the spacecraft. The RCS thrusters were also utilized to control spacecraft attitude during Trajectory Correction Maneuvers (TCMs) while the TCM main burns were executed by four TCM thrusters. Both the RCS and TCM thrusters were mounted onto the lander, extended through the backshell, and were scarfed to the contour of the backshell. Figure 1 depicts the nominal thruster vector of each RCS and TCM thruster, as shown in the spacecraft-fixed frame.

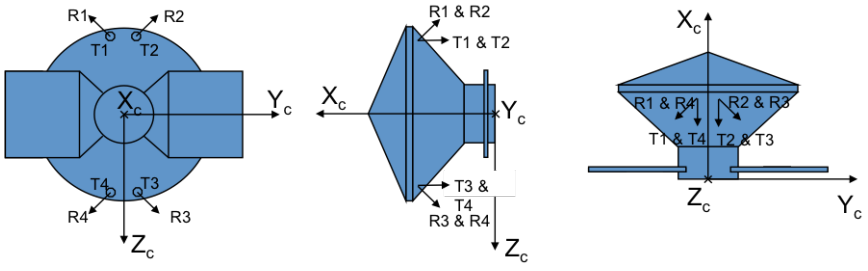

Figure 1. Thruster configuration, shown in the spacecraft-fixed frame.[8]

The RCS thrusters were designed to provide active 3-axis attitude control by firing in pairs. Each of the RCS thrust vectors had a non-zero component in all three spacecraft-fixed axes. As will be discussed in the next section, the nominal early cruise attitude relative to the Sun direction resulted in small spacecraft velocity changes (ΔV) in all three axes. In the nominal late cruise attitude profile, the Y-axis and Z-axis components were balanced while the X-axis component was not, imparting a ΔV along the X direction with every RCS thruster firing. To a lesser degree, velocity changes in the Y and Z directions also occurred as in reality the thrusters were not perfectly aligned and balanced.

Cruise Attitude Profile and Deadband Constraints

A cruise attitude profile was designed to balance various power, communications, and thermal constraints. In order to do so over the Earth-Sun-spacecraft geometry variation from launch to landing, separate attitude profiles were defined for early and late cruise. During early cruise, when the spacecraft was closer to the sun and thermal constraints drove the attitude design, the -X vector (solar array normal) was offset 50° from the Sun while the +Y vector pointed towards Earth and within the Earth-spacecraft-Sun plane (Figure 2). As the spacecraft traveled further from the Sun, the thermal constraint was loosened and the attitude design was driven by communication with the MGA. During late cruise, the -X vector was offset 2° from the Sun and the MGA boresight vector was pointed towards the Earth as much as possible (Figure 3). The transition from early to late cruise attitude occurred on July 12, 2018. (Note that the LGA was used for communication from launch to August 7, 2018, at which point primary communications were switched to the MGA. Limited communication via the LGAs occured during TCMs.)

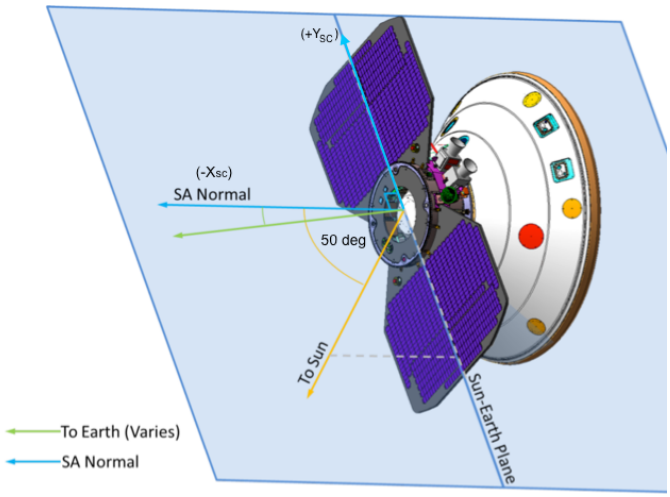

Figure 2. Early cruise attitude profile (launch to July 12, 2018).[8]

Adherence to the nominal cruise attitude profiles was ensured via attitude deadbanding. Two deadband strategies, summarized in Table 1, were defined to cover the variation in the Sun-Earth-spacecraft angle and the Earth and Sun ranges throughout the cruise to Mars. The spacecraft attitude was allowed to drift through a pre-defined three-dimensional deadband, with the RCS thrusters firing when a deadband limit was approached in order to keep the attitude inside the deadband. Tighter deadbands required more frequent RCS thruster firings to constrain the spacecraft attitude; as such, there was an increase in the imparted ΔV after the transition to the late cruise profile.

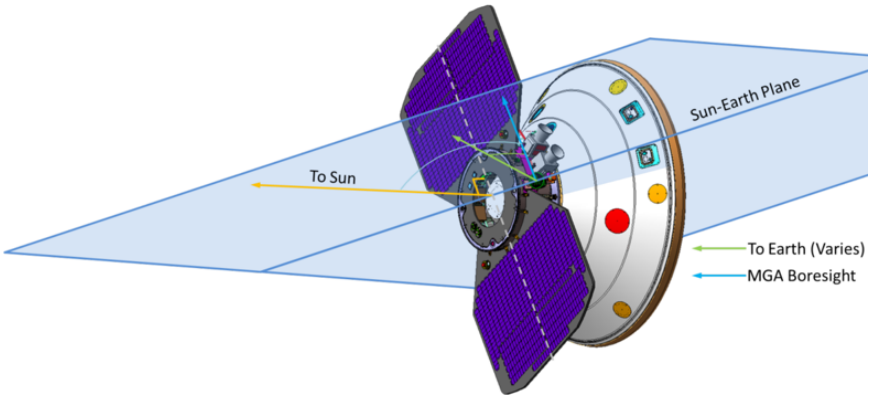

Figure 3. Late cruise attitude profile (July 12, 2018 to entry).[8]

Table 1. Spacecraft Attitude Deadband Definitions (Spacecraft-Fixed Frame)

Cruise Phase	X	Y	Z
Early Cruise (May 5, 2018 to July 12, 2018)	10°	10°	7.5°
Late Cruise (July 12, 2018 to November 26, 2018)	4°	4°	4°

ACS Telemetry

As discussed in Reference 9, the integrated effect of the many RCS thruster firings significantly altered the spacecraft trajectory and associated trajectory knowledge, and thus had to be properly handled in the orbit determination filter. *A priori* models of the small forces and attitude were provided throughout cruise via ACS telemetry. The flight system recorded a telemetry packet with thruster information every time an RCS or TCM thruster pulse was fired. The telemetry included the thruster on time, the pulse length, thruster number, on-board estimated ΔV, and on-board estimated attitude quaternions at the time of the thruster firing. This raw telemetry was downlinked and converted into discrete spacecraft attitude and impulsive thruster firings, which were in turn input into the orbit determination and trajectory prediction models. The average latency in receiving the ACS telemetry was approximately 30 minutes throughout cruise. In addition to the raw telemetry, filtered telemetry that had been processed by the onboard ACS filter was available; this filtered telemetry was utilized during the thruster calibration analysis.

RCS THRUSTER FLIGHT PERFORMANCE

Prior to launch, it was anticipated that during early cruise thrusters RCS1 and RCS4 would fire approximately 8 and 9 times per day, respectively. In contrast, RCS2 and RCS3 were predicted to fire approximately 29 and 30 times per day, respectively. This unbalanced effect was largely due to the thrusters compensating for solar torque while the solar arrays were pointing 50° off the Sun vector. (After the transition to late cruise, when the solar arrays were predominantly sun-pointed, the spacecraft dynamics were well-balanced and all thrusters were expected to fire roughly 23 times per day. The increase in firing frequency was driven by the tighter late cruise deadband requirements.) A complete history of the RCS thruster firings from launch to entry, as reported by the spacecraft, is shown in Fig 4. The figure denotes specific events which were accompanied by increased thruster activity, such as TCMs and the thruster calibration (TCAL).

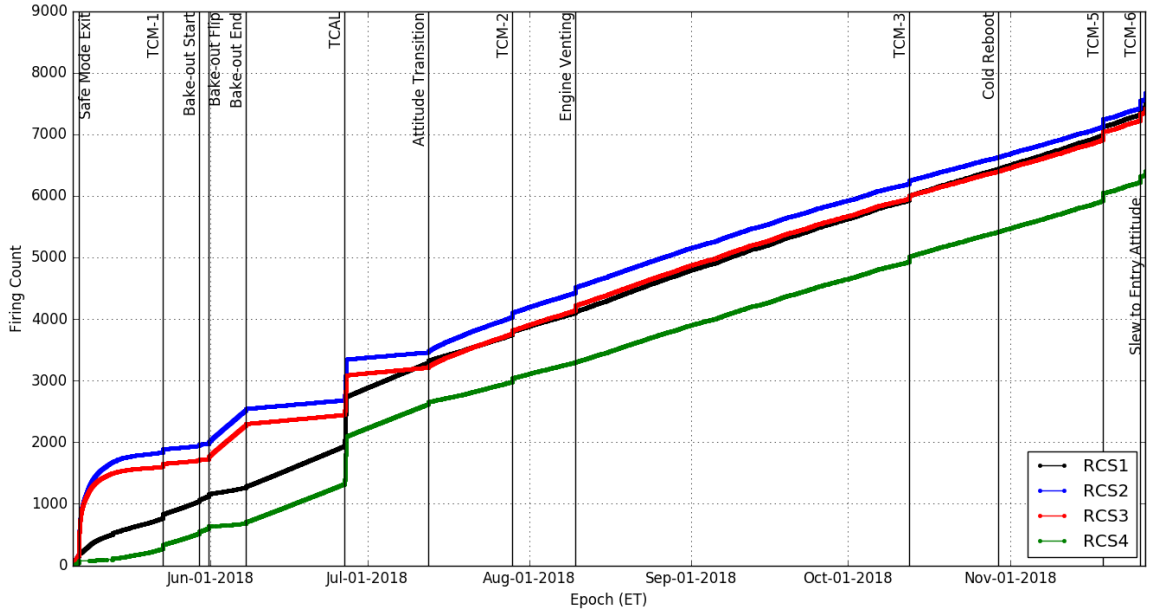

Figure 4. Complete count of RCS thruster firings and relevant spacecraft events.

Immediately following launch, the spacecraft experienced a significantly high level of outgassing, likely due to its extended storage when the launch was postponed from March 2016 to May 2018. Post-storage bakeout was not performed; as such, any atmospheric constituents absorbed by the spacecraft during its extended time in the clean room were expelled upon exposure to vacuum. In order to compensate for this outgassing immediately post launch, the RCS thrusters fired at approximately 25 times the level expected. As a result, TCM-1 was postponed until the outgassing in the early cruise attitude had largely dissipated and the associated predicted trajectory uncertainty had decreased. In order to avoid additional outgassing during the thruster calibration or after rotation to the late cruise attitude profile, which could negatively impact the TCM-2 design, execution, and assessment, an in-flight bakeout was performed just after TCM-1. The in-flight bakeout was executed by first allowing the spacecraft to finish out-gassing in the early cruise attitude, then the spacecraft was rotated to two of the TCAL attitudes in order to allow surfaces that would be exposed to the sun during the thruster calibration time to outgas. Following the bakeout, the spacecraft returned to its early cruise attitude. As shown in Figure 4, the outgassing following the transition to the late cruise attitude profile dissipated quickly relative to the initial post-launch out-gassing, and the RCS thruster firing rate was consistent with the expected rate throughout the remainder of cruise.

To illustrate the effect of the early cruise outgassing on the spacecraft attitude, Figures 5 and 6 present the telemetry-reported spacecraft attitude errors (in the spacecraft-fixed frame) over two-day spans in May and June 2018. In both May 2018 (Figure 5, 2 days post launch) and June 2018 (Figure 6, 6 weeks post launch), the spacecraft was in its early cruise attitude configuration. The nominal early cruise spacecraft attitude was canted 50° off the Sun direction, resulting in a solar pressure-induced torque about the Z axis. Contrasting this effect, the outgassing torque effectively pinned the spacecraft against its -Y and -Z deadband limits. As the solar torque and outgassing torque acted in opposite directions with the outgassing dominating, the solar torque effect was not

observable until the outgassing effectively dissipated. This “flipping” from the -Z-axis to +Z-axis is clearly illustrated in Figure 7, which shows the telemetry-reported Z-axis attitude errors from May 07, 2018 (2 days post launch) to May 25, 2018. The spacecraft attitude was pinned to the -Z limit during heavy outgassing, oscillated between the positive and negative limits when lighter out-gassing was balanced with solar torque, and finally flipped to the +Z limit when dominated by the solar torque.

Figure 8 shows the telemetry-reported attitude errors after the transition to the late-cruise attitude configuration. For the remainder of cruise, the spacecraft X-axis was pointed towards the sun, resulting in a spacecraft that was balanced in regards to the solar torque. The attitude errors drifted throughout the nominal deadbands in each axis, with the increased frequency of thruster firings due to the tighter deadband limits.

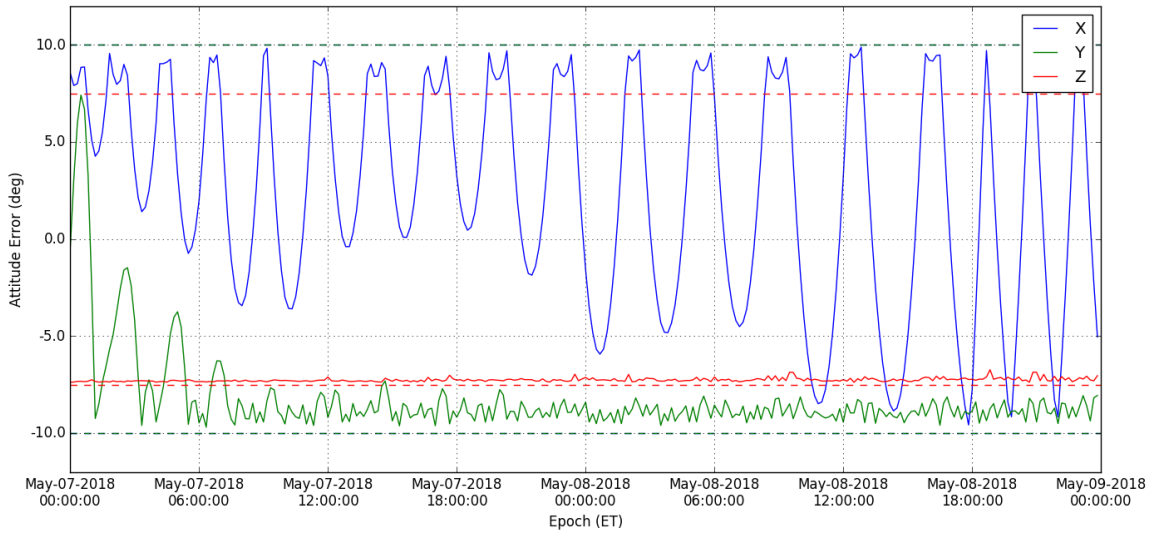

Figure 5. Spacecraft attitude error during heavy outgassing immediately post launch (deadbands denoted by dashed lines).

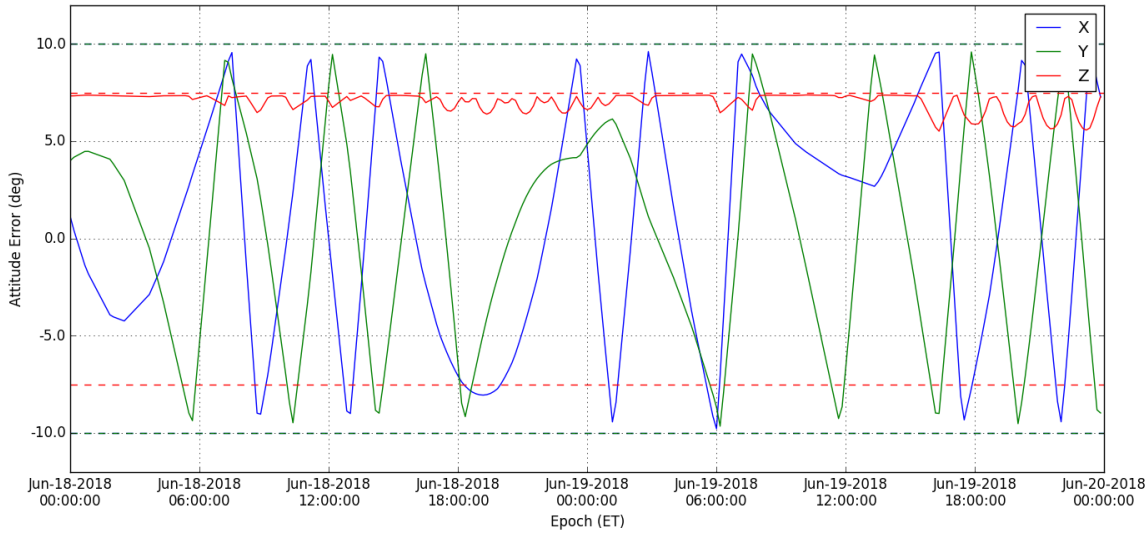

Figure 6. Spacecraft attitude error during nominal early cruise operations (deadbands denoted by dashed lines).

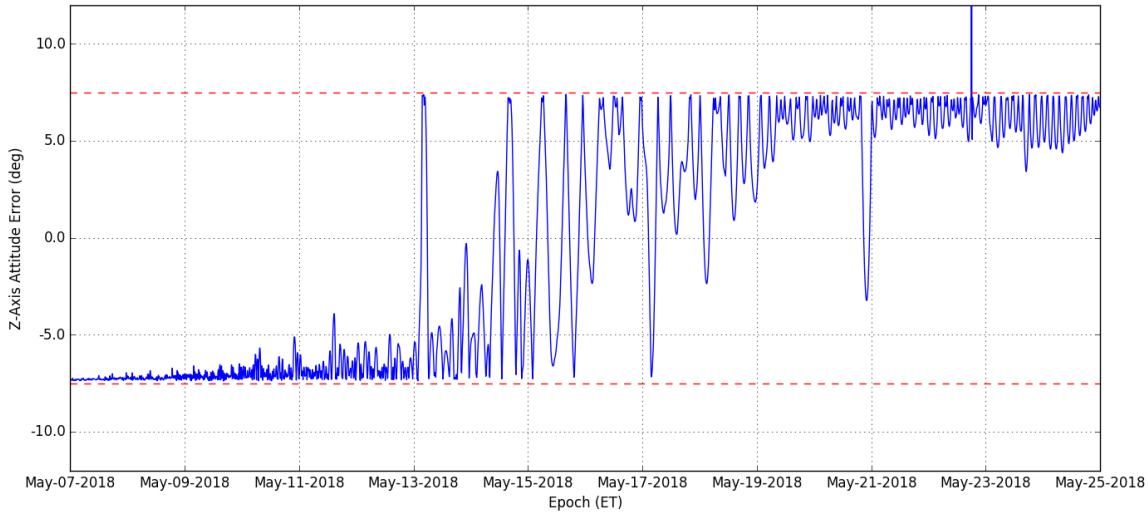

Figure 7. Z-axis spacecraft attitude error in response to post-launch outgassing and solar torque (deadband denoted by dashed lines).

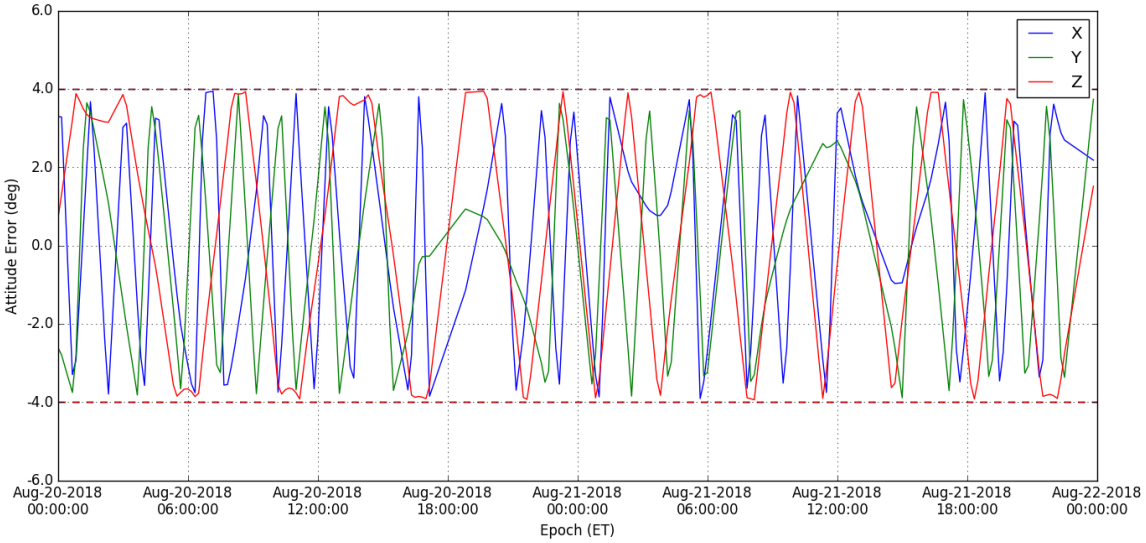

Figure 8. Spacecraft attitude error during nominal late cruise operations (deadbands denoted by dashed lines).

SMALL FORCE ESTIMATION AND PREDICTION STRATEGY

The orbit determination strategy accounted for errors in the small force telemetry within the data arc, and predicted the future RCS thruster performance from the data cut off to time of entry.[9] Though the InSight ACS design was based on Phoenix heritage, the approach used by the InSight navigation team differed significantly from that used to navigate the Phoenix spacecraft.

The Phoenix model captured the combined effect of the individual RCS thrusters via estimating the overall long-term constant and short-term stochastic spacecraft-fixed accelerations due to the small forces.[1] The InSight model expanded upon this design by reconstructing the behavior of each individual RCS thruster within the data arc, and predicting the future average acceleration per thruster.[9] Prior to the thruster calibration event, the thruster directions and the velocity change (ΔV) per firing were defined for each RCS thruster using the pre-launch nominals. After the thruster calibration, the thrust vector directions and magnitude were updated to the estimated values. By ingesting the ACS on-board telemetry, nominal impulsive velocity changes and spacecraft quaternions were modeled at the time of each thruster firing. The filter was configured to estimate thruster pointing offsets and a scale factor on the nominal ΔV magnitude. Additional, stochastic errors in the ΔV magnitude were estimated for each individual thruster firing. The baseline small force filter configuration is summarized in Table 2.

Table 2. Baseline Small Force Estimation Strategy

Estimated Parameter (Per Thruster)	Model	*A Priori* Value	*A Priori* Uncertainty
Thrust Direction Y Offset	Bias	0°	3°
Thrust Direction Z Offset	Bias	0°	3°
ΔV Magnitude	Bias	0%	3%
ΔV Magnitude	White Noise Stochastic	0%	15%

The propagation of the estimated spacecraft position and velocity to the entry interface point included predictions of the future small force behavior of each thruster. Early on, it was clear that empirically-determined thruster behavior would be necessary due to the dynamic outgassing response, which was not adequately captured by the pre-launch nominal models. Assuming nominal thruster performance and linearly fitting to recent histories of thruster firing counts as reported by the spacecraft (including only small force firings during nominal deadbanding), an empirical prediction of the future acceleration imparted by each thruster was computed for each orbit determination solution. This empirical prediction was in turn scaled by the estimated thrust magnitude scale factor to account for errors in the nominal thruster performance assumption. In effect, this effort was an on-going thruster calibration that characterized the short-term deadbanding behavior in response to varying astrodynamic conditions. Early in cruise, the short-term variation in the empirical predictions was significant due to the spacecraft outgassing (Figure 4). By late cruise and final approach, the day-to-day variation was less than 0.5 mm/sec over a one day prediction. The impact of the predicted small forces on the Mars entry point was directly proportional to the time from the end of the orbit determination data arc to Mars entry, and as such even small short-term variations early in cruise generated large entry point differences.

Figures 9, 10 and 11 present a comparison of the orbit determination performance using various small force models. Each figure shows the solution as propagated from the data cut off to the Mars entry B-plane, and together represent the changing importance of the small force modeling techniques throughout cruise. Figure 9 was generated at the TCM-2 data cut off (July 07, 2018), and Figure 10 was generated at the TCM-3 data cut off (October 07, 2018); the data arc for both sets began on June 07, 2018. The solutions shown in Figure 11 included data from just after TCM-3 (October 12, 2018) to the TCM-6 data cut off (entry minus 48 hours). In addition to the baseline filter configuration, variations include increasing and decreasing the predicted small force accelerations by 5% and a simplified Phoenix-like acceleration model (denoted in the legend as "sf_predict_increase", "sf_predict_decrease", and "phx_accel", respectively). The Phoenix-like model estimated constant and stochastic accelerations in the spacecraft frame to account for the combined effect of the four RCS thrusters. As implemented, this model did not ingest the small force and attitude telemetry; as such, the *a priori* uncertainties on the spacecraft-fixed accelerations were on the order of the pre-launch nominal values.

At the time of the TCM-2 data cut off, the solution uncertainty was driven largely by the data uncertainties and the propagated solution was not significantly sensitive to the 5% variations in predicted small force accelerations. However, there was significant sensitivity to the Phoenix-like acceleration model, which predicted an entry interface point that is more than 3-σ away from the baseline. Note that prefit Doppler and range residuals consistently indicated that the baseline approach predicted the true trajectory quite well, whereas the prefit residuals generated with the Phoenix-like approach began to deviate soon after the data cut off.[9]

By the TCM-3 data cut off three months later, the various small force models began to converge to the same entry interface point and the solution uncertainty was dominated by uncertainty in the predicted small force accelerations. The 5% variations in the predicted small forces, which conservatively bounded the observed daily variations in the RCS thruster performance, shifted the entry interface point by approximately 1-σ. The Phoenix-like model produced a solution that is statistically consistent with the baseline approach, though with significantly larger uncertainty. By the time of final Mars approach, the orbit determination solutions produced by the small force model variations were indistinguishable due to the decreased propagation time to entry (Figure 11).

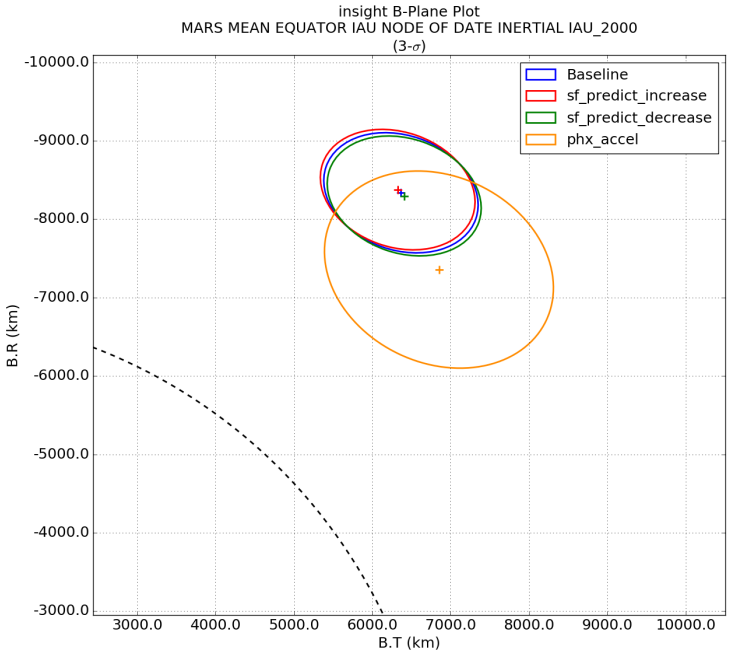

Figure 9. Comparison of small force models at the TCM-2 data cut off (July 07, 2018). Dashed line denotes Mars impact radius.

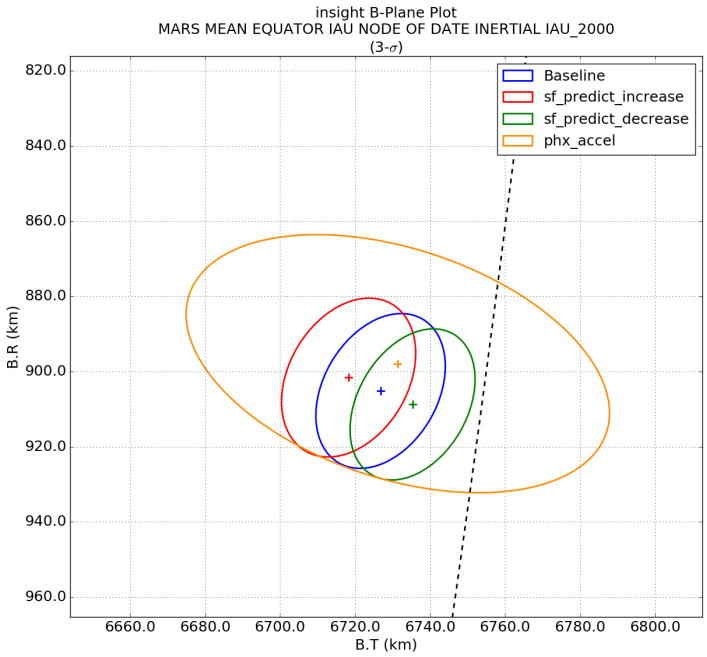

Figure 10. Comparison of small force models at the TCM-3 data cut off (October 07, 2018). Dashed line denotes Mars impact radius.

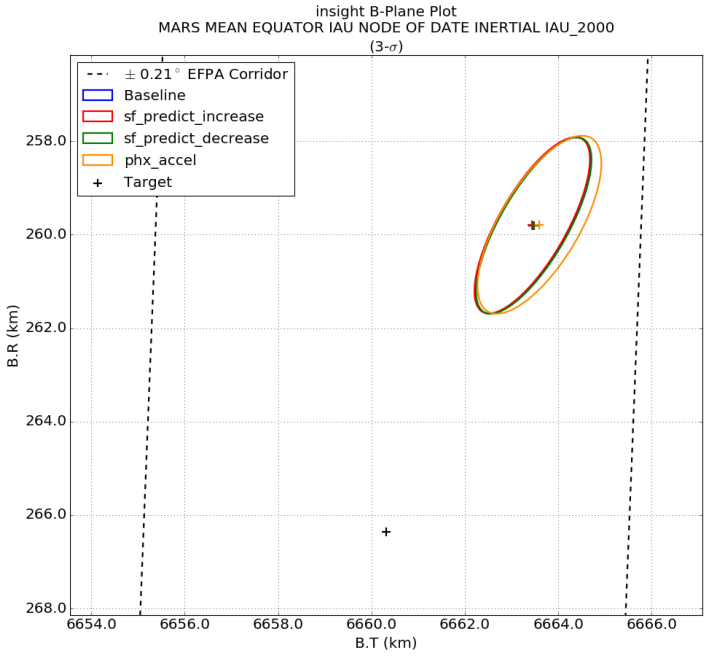

Figure 11. Comparison of small force models at the TCM-6 data cut off (Entry - 48 hours). Dashed lines denote entry flight path angle requirement.

THRUSTER CALIBRATION

As discussed in Reference 9, ACS propulsion system activity was the driving error source in the entry flight path angle delivery. The dominant errors were due to attitude slew prediction errors during the TCMs, with the cruise deadbanding attitude control contributing to a lesser but still significant level. Given the need to accurately model the true thruster performance, empirically-determined short-term linear trends were used to predict future RCS thruster small forces. Additionally, an in-flight thruster calibration was executed in an attempt to better characterize the effective thrust vector of each RCS thruster.

Thruster Calibration Overview

Though the InSight spacecraft carried significant design heritage from past Mars missions, the construction of each new propulsion system is unique and hence differs from its predecessors. Furthermore, the flight experience of the heritage ACS systems does not provide full understanding of the deadbanding response. No explicit thruster calibration activity was performed for Mars Polar Lander, and empirical estimations of the thrust vectors during cruise did not agree well with pre-launch nominal vectors.[10] The Phoenix thruster calibration, which improved the RCS thrust vectors and magnitudes by about 6%,[7] was updated for the InSight activity to allow calibration of single thrusters instead of thruster pairs and full observability from the line-of-sight Doppler measurements.

The thruster calibration activity was designed by the Lockheed Martin InSight ACS team, in concert with JPL.[8] The selection of the thruster calibration epoch on June 26, 2018 was driven by the Sun-spacecraft-Earth angle and other spacecraft activities during cruise. Four spacecraft attitudes

were selected to maximize observability of the thruster activity via the line-of-sight Doppler data while maintaining attitude safety constraints. The four attitudes are shown relative to the spacecraft-fixed frame in Figure 12. During the thruster calibration activity, nine consecutive sets of 16 pre-defined minimum impulse thruster pulses were performed at each of the four attitudes, with the nominal attitude reset between sets. The cumulative effort included 144 calibration pulses per thruster (576 calibration pulses in total). The order of the thruster firings per set, also referred to as the pulse train, was 3, 3, 2, 2, 4, 4, 1, 1, 2, 2, 3, 3, 1, 1, 4, 4 as shown in Figure 13. There was a 10 second hold between firings of the same thruster, and a 50 second hold before switching to the next thruster. The thruster calibration duration was approximately 8 hours, with a breakdown of the timeline (per attitude) shown in Table 3. The design of the 16 pulses provided observability of each individual thruster, rather than thruster pairs. Repeating the 16-impulse set nine times increased the signal-to-noise ratio of the observations. While the visibility into the individual thruster geometry and behavior was optimized by the implemented thruster calibration, it must be noted that the pulse trains were not representative of nominal deadbanding behavior. The thrusters fired much more frequently during the thruster calibration than nominal deadbanding, and temperature-driven variations may have impacted both the effective thrust direction and magnitude. The calibration data was filtered to include only minimum impulse bit firings, which is more reflective of routine deadbanding. The thruster calibration activity as performed had limited applicability when applied to nominal deadbanding, particularly when daily small force trending was performed.

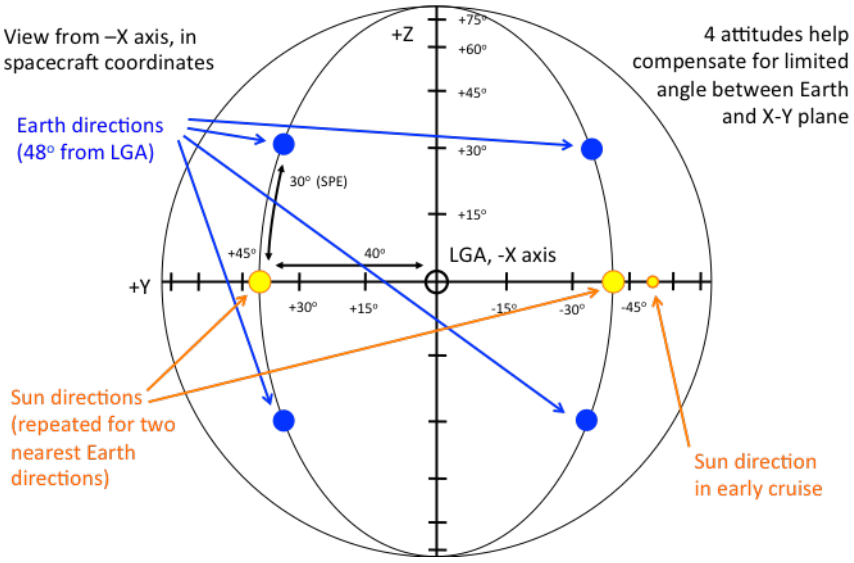

Figure 12. InSight thruster calibration attitudes.[8]

Filter Configuration

The analysis utilized an Unscented Kalman Filter/Smoother, which is better suited to system non-linearities than the conventional linear Kalman Filter utilized for the standard orbit determination.[11,12] As the primary objective was to characterize the impulsive $\Delta\vec{V}$ imparted by each thruster, the filter states included each thruster's effective linear impulse vector ($\vec{p}$). Additional filter states required to fit the data included the spacecraft quaternions and angular rates (estimated as dynamic parameters), a constant solar torque (to account for mismodeling in the orbit determination solution), and an offset in the spacecraft center of mass location.

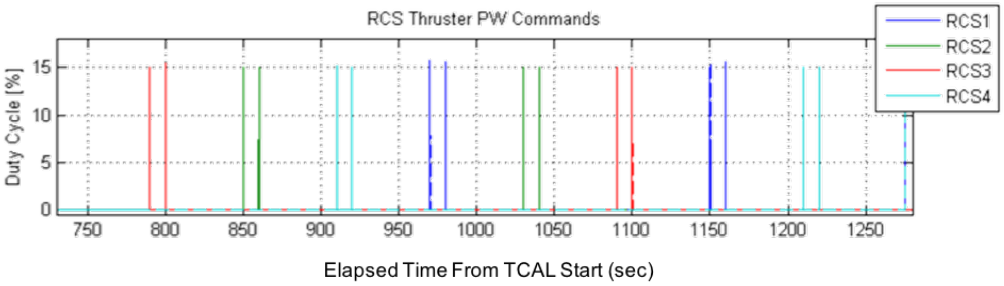

Figure 13. Thruster calibration pulse train.[8]

Table 3. Thruster Calibration Timeline of Events (Repeats at each calibration attitude)

Activity	Duration
Slew to calibration attitude	12 minutes
Execute calibration block (x9)	
Wait for pre-burn Doppler acquisition	1 minute
Fire pulse train sequence	8 minutes
Wait for post-burn Doppler acquisition	50 seconds
Attitude reset (x8)	3 minutes
Slew to nominal cruise attitude (after fourth attitude)	12 minutes

Multiple data streams were utilized to enhance the quality of the thruster calibration. The standard channelized telemetry included the spacecraft quaternions and angular velocity ($\Delta\vec{\omega}$) data at 5 Hz, while the MIMU provided 50 Hz angular velocity data over the pulses. The high frequency MIMU data provided additional visibility into the angular velocity change across each single pulse. Increased visibility into the line-of-sight velocity was provided by Doppler tracking data. As shown by Eq. 1, the angular momentum change $\Delta\vec{H}$ linearly relates the angular velocity to the linear impulse vector. (I and $S()$ denote the moment of inertia and skew symmetric operator, respectively.) However, there exists an ambiguity in the resolution of the moment arm from the center of mass to the thruster location ($\vec{r}$). The additional constraint needed to fully estimate the linear impulse vector is provided via the linear momentum, which linearly relates the linear impulse to the spacecraft mass (m) and imparted velocity change (Eq. 2). The line-of-sight ($\bar{l}$) velocity component is directly observable via Doppler tracking data. Combining the angular and linear momentum equations results in a well-determined system in which the linear impulse $\vec{p}$ can be estimated from the angular velocity and Doppler tracking data (Eq. 3).

$$\Delta\vec{H} = I\Delta\vec{\omega} = \vec{r}\times\vec{p} = S(\vec{r})\vec{p} \tag{1}$$

$$\vec{p} = m\Delta\vec{V} \tag{2}$$

$$\begin{bmatrix} S(\vec{r}) \\ \bar{l}^T \end{bmatrix}\vec{p} = \begin{bmatrix} I\Delta\vec{\omega} \\ m(\bar{l}\cdot\Delta\vec{V}) \end{bmatrix} \tag{3}$$

While standard cruise orbit determination typically uses 10-second or 60-second Doppler tracking data, the calibration used 1-second Doppler to improve short-term observability. Note that in order to be useful for thruster calibration, all dynamic and observable errors except those due to the thruster firings must be removed from the Doppler data. This was achieved by pre-processing the raw Doppler data with the trajectory solution produced by the Navigation team, which included high-fidelity models of the dynamic perturbations, observables, and spacecraft models. The filtered Doppler observables were then converted from two-way X-band frequency into line-of-sight ΔV.

Thruster Calibration Results

The data corresponding to each of the nine pulse trains was filtered separately, with the results then combined in a statistical batch sense to produce an overall estimate of the thrust direction and magnitude. The postfit residuals for the quaternion, angular rate, and line-of-sight ΔV data from the first pulse train, shown in Figures 14 through 16, represent typical filter performance. The quaternion residuals (Figure 14) include systematic trends consistent with star tracker measurement errors. The angular rate residuals (Figure 15) are largely white noise, but exhibit two distinct uncertainty levels corresponding to the low-rate channelized telemetry (lower measurement noise) and the high-rate MIMU data (higher measurement noise). The line-of-sight velocity residuals (Figure 16) are white noise at a level statistically consistent with 2-way X-band Doppler data.

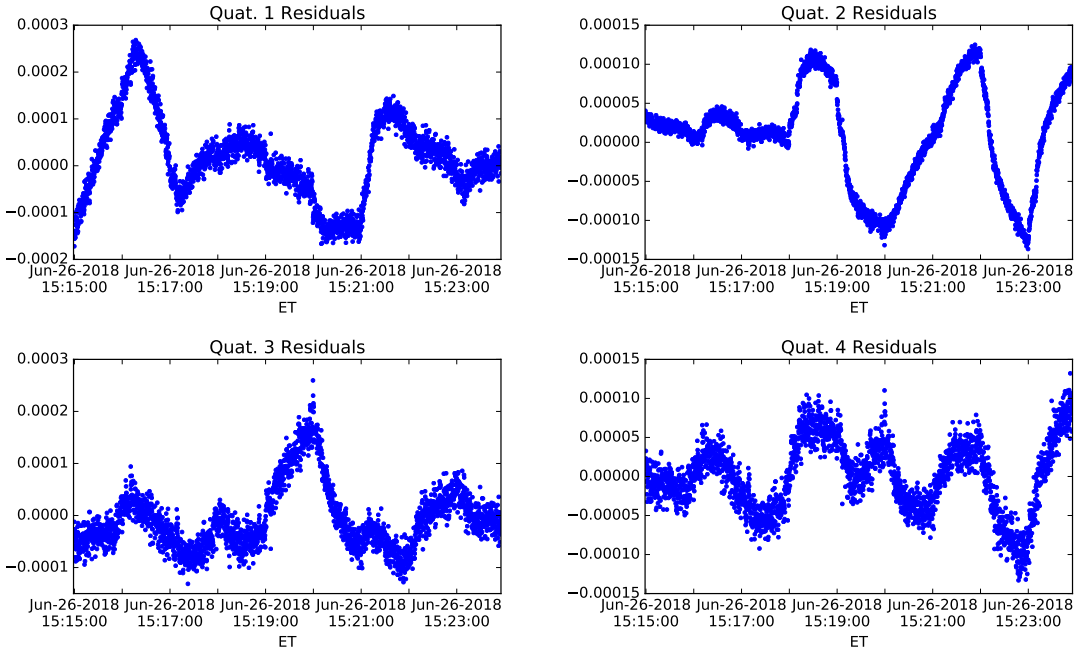

Figure 14. Postfit quaternion residuals for the first pulse train.

The estimated effective thrust directions (defined in the spacecraft-fixed frame) and magnitude scale factors for each thruster are shown in Table 4, along with the pre-launch nominal thrust directions. Substantial offsets in the thrust direction were estimated for each of the thrusters; though the uncertainty on the pre-launch nominal thrust directions was 3°, the thruster calibration filter shifted the vector directions by up to 13.5°. Significant adjustments to the ΔV magnitude were also observed, as the scale factors were estimated to 65% to 75% of the pre-launch nominals.

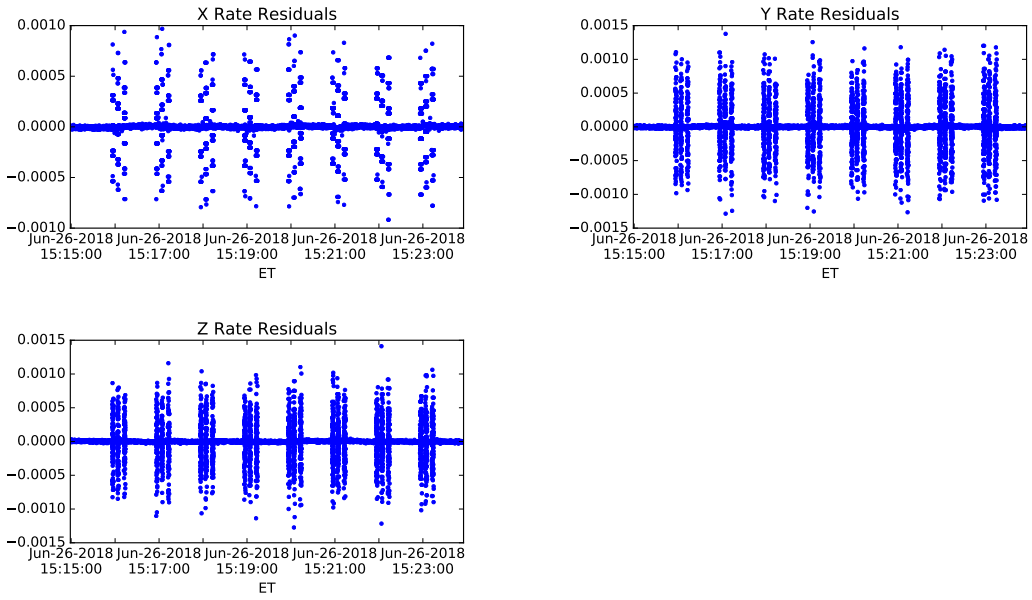

Figure 15. Postfit angular rate residuals for the first pulse train.

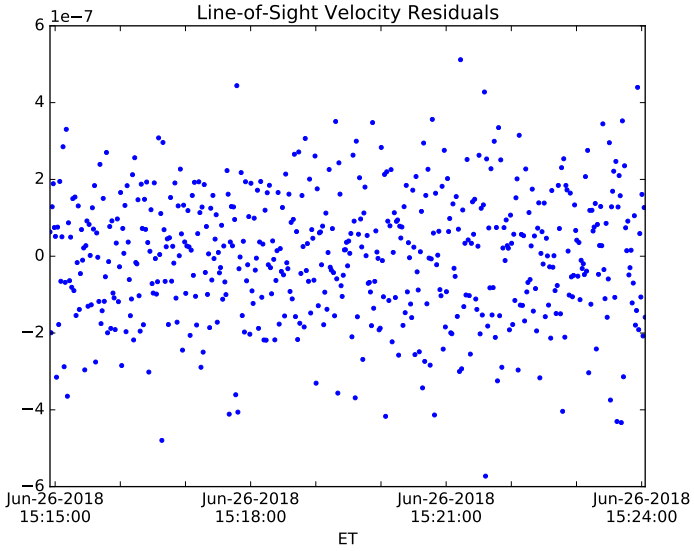

Figure 16. Postfit line-of-sight ΔV residuals for the first pulse train.

The impact of applying the calibrated thruster parameters is shown in Figure 17, which portrays the orbit determination solution from October 5, 2018 propagated to the Mars entry B-plane. Prior to the thruster calibration, it was observed that the orbit determination filter adjusted the nominal thrust directions up to 5° and scaled the thrust magnitude by up to 8%. After applying the calibrated thruster directions and magnitude scales and re-running the orbit determination filter, the thrust magnitudes were adjusted by less than 3% but there was no improvement to the thrust direc-

Table 4. Estimated Thruster Magnitude Scale Factor and Direction ([X, Y, Z])

	RCS1	RCS2
Nominal Direction	[0.3404, 0.7411, 0.5786]	[0.3652, -0.7571, 0.5417]
Estimated Direction	[0.4722, 0.7642, 0.4394]	[0.3610, -0.8002, 0.4790]
Estimated Direction Offset	11.08°	4.367°
Estimated Scale Factor	0.6738	0.7525
	RCS3	**RCS4**
Nominal Direction	[0.3707, -0.7661, -0.5251]	[0.3308, 0.7493, -0.5736]
Estimated Direction	[0.5176, -0.6997, -0.4925]	[0.4922, 0.7713, -0.4036]
Estimated Direction Offset	9.434°	13.52°
Estimated Scale Factor	0.6536	0.6900

tion estimation. Applying the thruster calibration shifts the entry interface point by approximately 1-σ relative to the baseline (pre-launch nominal) solution. The uncertainty ellipse is significantly reduced, as the propagated uncertainty is directly proportional to the predicted small force accelerations and thus directly proportional to the estimated thruster magnitude scale factors. As the thruster calibration activity did present an improvement in the knowledge of the magnitude of the small force firings, the baseline orbit determination approach was updated to include the calibrated thruster parameters.

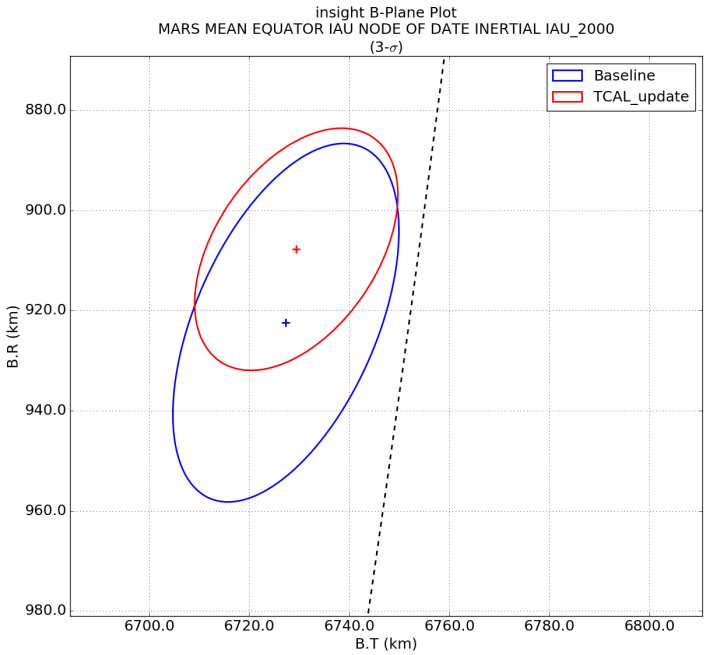

Figure 17. Effect of thruster calibration on late-cruise trajectory solution.

SUMMARY

As was the case with previous missions that have flown similar spacecraft buses, proper characterization of the InSight spacecraft's unbalanced attitude control thruster system was paramount to the successful Mars landing. The thruster calibration campaign performed on June 26, 2018, was designed to maximize observability into the three dimensional thrust vector produced by each of the four RCS thrusters. The empirical reconstruction of the effective thrust vectors and associated thrust magnitude via spacecraft quaternion, angular rate, and Doppler tracking data improved the characterization of the thrust magnitude but had limited utility in determining the thrust vector offsets. The nature of the thruster calibration sequence is such that the calibration data is not representative of nominal cruise attitude deadbanding. The baseline orbit determination approach, which used empirical trending to recent small force telemetry and estimated corrections to nominal thruster models to predict future thruster accelerations, produced solutions that were stable, statistically consistent, and predicted the spacecraft trajectory exceptionally well.

ACKNOWLEDGEMENTS

The authors would like to thank Tim McElrath (Jet Propulsion Laboratory, Mission Design and Navigation) for his expertise and experience, both of which provided great insight into the spacecraft ACS response.

The work described in this paper was carried out at the Jet Propulsion Laboratory, California Institute of Technology, under a contract with the National Aeronautics and Space Administration.

REFERENCES

[1] M. S. Ryne, E. Graat, R. Haw, G. Kruizinga, E. Lau, T. Martin-Mur, T. McElrath, S. Nandi, and B. Portock, "Orbit Determination for the 2007 Mars Phoenix Lander," AIAA/AAS Astrodynamics Specialist Conference and Exhibit, Honolulu, HI, USA, 2008.

[2] P. Antreasian, D. Baird, J. Border, P. Burkhart, E. Graat, M. Jah, R. Masa, T. McElrath, and B. Portock, "2001 Mars Odyssey Orbit Determination During Interplanetary Cruise," *Journal of Spacecraft and Rockets*, Vol. 42, May 2005.

[3] T. You, E. Graat, E. Halsell, D. Highsmith, S. Long, R. Bhat, S. Demcack, E. Higa, N. Mottinger, and M. Jah, "Mars Reconnaisance Orbiter Interplanetary Cruise Navigation," *Proceedings of 20th International Symposium on Space Flight Dynamics*, Anapolis, MD, September 2007.

[4] B. Kennedy, E. Carranza, and K.Williams, "1-AU Calibration Activities for Stardust Earth Return," *Proceedings of the AAS/AIAA Space Flight Mechanics Meeting*, Maui, HI, February 2004.

[5] S. Nandi, B. Kennedy, K. Williams, and D. Byrnes, "On-Orbit Maneuver Calibrations for the Stardust Spacecraft," *Proceedings of the AIAA/AAS Astrodynamics Specialist Conference*, Keystone, CO, August 2006.

[6] A. Stephenson, D. Mulville, F. Bauer, G. Dukeman, P. Norvig, L. LaPiana, P. Rutledge, D. Folta, and R. Sackheim, "Mars Climate Orbiter Mishap Investigation Board Phase I Report," tech. rep., National Aeronautics and Space Administration, November 10 1999.

[7] M. E. Lisano, G. Kruizinga, and B. Portock, "The NASA Phoenix 2007 Mars Lander Thruster Calibration Estimator: Design and Validation," AIAA/AAS Astrodynamics Specialist Conference and Exhibit, Honolulu, HI, USA, 2008.

[8] A. Halsell, F. Abilleira, M.-K. Chung, E. Gustafson, K. Fujii, Y. Hahn, D. Jefferson, G. Kruizinga, E. Lau, J. Lee, S. E. McCandless, N. Mottinger, J. Seubert, and M. Wallace, "InSight Navigation Plan (2018 Baseline), Revision C," March 2018.

[9] E. D. Gustafson, C. A. Halsell, D. Jefferson, E. Lau, J. Lee, S. E. McCandless, N. Mottinger, and J. Seubert, "InSight Orbit Determination," AAS/AIAA Space Flight Mechanics Meeting, Ka'anapali, HI, January 2018.

[10] T. McElrath, "Mars Polar Lander (MPL) Small Forces File Modeling Development," Internal JPL Memorandum 312/00.A- 005, Jet Propulsion Laboratory, March 2000.

[11] S. Julier and J. Uhlmann, "A New Extension of the Kalman Filter to Nonlinear Systems," *SPIE 3068 Signal Processing, Sensor Fusion and Target Recognitions*, Vol. VI, July 1997.

[12] B. Tapley, B. Schutz, and G. Born, *Statistical Orbit Determination*. 200 Wheeler Road, Burlington, MA, 01803: Elsevier Academic Press, 2004.